Bulk observables in Pb + Pb collisions at $\sqrt{s_{NN}} = 5.02$ TeV at the CERN Large Hadron Collider within the integrated hydrokinetic model

V. M. Shapoval[1] and Yu. M. Sinyukov[1,2]

[1]*Bogolyubov Institute for Theoretical Physics, 03143 Kiev, Ukraine*
[2]*Tomsk State University, Department of Physics, Tomsk 634050, Russia*

The paper is devoted to the description and prediction of various bulk observables in the Pb + Pb collisions at the Large Hadron Collider energy $\sqrt{s_{NN}} = 5.02$ TeV within the integrated hydrokinetic model (iHKM). Sensitivity of the results to the choice of the appropriate model parameter values is also investigated. It is found that changing of the relaxation time and the rate of thermalization, which characterize the prethermal stage of the matter evolution, as well as switching to another equation of state at the hydrodynamic stage and the corresponding hadronization temperature, does not destroy the results if simultaneously one provides an appropriate adjusting of the initial time for the superdense matter formation and related maximal initial energy density.

I. INTRODUCTION

The realistic simulation of a relativistic heavy-ion collision, which allows to describe or predict a wide variety of measured bulk observables, requires a complicated model consisting of several components, each of them describing a certain stage of the collision in the most appropriate approach.

According to this requirement, the well-known integrated hydrokinetic model (iHKM) model [1,2] consists of a set of modules/stages, corresponding to a series of successive phases of system's evolution process, including formation of superdense matter, its gradual thermalization, viscous relativistic hydrodynamic expansion as continuous medium, particlization, and the hadronic cascade stage. The "development" of the system at each stage is regulated by specific model parameters, and the aggregated effect of the matter's evolving during all the stages defines the final state of the system and the behavior of various observables, measured in the experiments.

Naturally, a researcher is interested in finding the connection between different parameter values and the simulation results in order to have the possibility to better understand the nature of the investigated processes and to discover the properties and characteristics of hot dense matter, basing on the experimental data.

In Refs. [1,2] the influence of different iHKM parameters (such as initial energy-density profile shape and its

momentum anisotropy, shear viscosity at the hydrodynamical stage etc.) on the obtained results for spectra, v_2 coefficients, interferometry radii, etc., was already studied in application to Pb + Pb collisions at the Large Hadron Collider (LHC) energy $\sqrt{s_{NN}} = 2.76$ TeV.

In the present paper we are aiming to investigate the dependence of our simulation results on such parameters as thermalization and relaxation times at the prethermal stage, τ_{th} and τ_{rel}, at the LHC energies, and the particlization/hadronization temperatures T_p, associated with the different equations of state, giving ourselves a task to predict/describe a set of bulk observables in the LHC Pb + Pb collisions at the higher energy $\sqrt{s_{NN}} = 5.02$ TeV.

II. RELAXATION RATE AND THERMALIZATION TIME IN THE LHC COLLISIONS WITHIN IHKM

The expansion of thermalized continuous medium near local thermal and chemical equilibrium is described in iHKM on the basis of the relativistic viscous hydrodynamics approximation in the Israel-Stewart formalism. This stage of the system's evolution is characterized by the shear viscosity parameter, η/s. As it was found in Ref. [1], this parameter for quark-gluon matter should have the value close to the minimal possible one, $1/4\pi \approx 0.08$. The initial conditions for hydrodynamical evolution of the system are formed during the prethermal stage, which models the transformation of initially nonthermalized system into thermalized one [2]. The dynamics of the system's expansion at the prethermal stage is described within the energy-momentum transport approach in relaxation time approximation [1].

At the initial proper time τ_0 the system's energy-momentum tensor $T_0^{\mu\nu}(x)$ has the nonhydrodynamic and nonthermal structure which is formed as discussed below. A gradual hydrodynamization of the system at the prethermal

evolution stage is accompanied by the corresponding smooth transformation of the energy-momentum tensor, so that at the thermalization time τ_{th} it reaches the Israel-Stewart viscous hydrodynamics form $T^{\mu\nu}_{\text{hydro}}(x)$. At intermediate times, between τ_0 and τ_{th}, the system's energy-momentum tensor can be presented within the relaxation-time approximation for Boltzmann equation [3] as

$$T^{\mu\nu}(x) = T^{\mu\nu}_{0,\text{free-evolving}}(x)\mathcal{P}(\tau) + T^{\mu\nu}_{\text{hydro}}(x)[1 - \mathcal{P}(\tau)]. \quad (1)$$

The matter evolution is determined by the following equations:

$$\partial_\mu\{[1 - \mathcal{P}(\tau)]T^{\mu\nu}_{\text{hydro}}(x)\} = -T^{\mu\nu}_{0,\text{free-evolving}}(x)\partial_\mu\mathcal{P}(\tau). \quad (2)$$

To arrive at the hydrodynamical tensor $T^{\mu\nu}_{\text{hydro}}(x)$ at $\tau = \tau_{\text{th}}$ one should require

$$\mathcal{P}(\tau_0) = 1, \quad \mathcal{P}(\tau_{\text{th}}) = 0, \quad \text{and} \quad \partial_\mu\mathcal{P}(\tau_{\text{th}}) = 0. \quad (3)$$

Equations (2) can be considered the equations of relativistic hydrodynamics for the modified energy-momentum tensor $\tilde{T}^{\mu\nu}_{\text{hydro}}(x) = [1 - \mathcal{P}(\tau)]T^{\mu\nu}_{\text{hydro}}(x)$ with a "source" term on the right-hand side and rescaled energy density $\tilde{\epsilon} = [1 - \mathcal{P}(\tau)]\epsilon$ and pressure $\tilde{p} = [1 - \mathcal{P}(\tau)]p$. Here we also assume that the relaxation time $\tau_{\text{rel}}(x, p)$ for each fluid element is very close to that in its rest frame, $\tau^*_{\text{rel}}(x, p)$, and depends only on the proper time τ, so that the weight function $\mathcal{P}(\tau, \mathbf{r}, p) = \exp[-\int_{\tau_0}^{\tau} 1/\tau_{\text{rel}}(\tau', \mathbf{r}, p)d\tau']$ also depends only on τ:

$$\mathcal{P}(\tau) = \exp\left[-\int_{\tau_0}^{\tau} \frac{1}{\tau_{\text{rel}}(\tau')}d\tau'\right]. \quad (4)$$

Such an approximation corresponds to the Bjorken picture [4], in which the processes of matter thermalization are synchronous in proper time of the fluid elements, and the system's thermalization completes simultaneously with the beginning of its hydrodynamic expansion at the proper time τ_{th}.

Assuming further $\tau_{\text{rel}}(\tau') = \tau_{\text{rel}}(\tau_0)\frac{\tau_{\text{th}}-\tau'}{\tau_{\text{th}}-\tau_0}$, and performing the integration in Eq. (4), one readily obtains $\mathcal{P}(\tau) = (\frac{\tau_{\text{th}}-\tau}{\tau_{\text{th}}-\tau_0})^{\frac{\tau_{\text{th}}-\tau_0}{\tau_{\text{rel}}(\tau_0)}}$. The value of $\tau_{\text{rel}}(\tau_0) \equiv \tau_{\text{rel}}$ here is one of the iHKM parameters. From (3) it follows that one should have $(\tau_{\text{th}} - \tau_0)/\tau_{\text{rel}} > 1$.

Thus, the time parameters, determining the dynamics of the prethermal stage in iHKM, are the initial time τ_0, relaxation time τ_{rel}, and thermalization time τ_{th}. The first one defines the proper time, when the initial energy-density profile of strongly interacting matter is formed after overlapping of the colliding nuclei, the second one is related to the rate of transformation of the system from the initial nonequilibrium state to the hydrodynamical one, and the third parameter defines the time when the system becomes nearly thermal.

The initial prethermal states are constructed with the help of MC Glauber GLISSANDO code [5] and are regulated by the following model parameters: $\epsilon_0(\tau_0)$ (the initial maximal energy density in the center of the system at the starting proper time τ_0), α (the parameter defining the proportion between the contributions from "binary collisions" and "wounded nucleons" models into the initial energy-density profile), and Λ [regulating the momentum anisotropy of the initial parton distribution function $f_0(p)$]. The latter function in iHKM is

chosen to have the following form, consistent with color glass condensate (CGC) approach:

$$f_0(p) = g\exp\left[-\sqrt{\frac{(p \cdot U)^2 - (p \cdot V)^2}{\lambda^2_\perp} + \frac{(p \cdot V)^2}{\lambda^2_\parallel}}\right], \quad (5)$$

where $U^\mu = (\cosh\eta, 0, 0, \sinh\eta)$, $V^\mu = (\sinh\eta, 0, 0, \cosh\eta)$. In the rest frame of the fluid element one has $\eta = 0$, $(p \cdot U)^2 - (p \cdot V)^2 = p^2_\perp$ and $(p \cdot V)^2 = p^2_\parallel$, so the parameters $\lambda^2_\parallel$ and $\lambda^2_\perp$ can be associated with the two temperatures—one along the beam axis and another, orthogonal to it, correspondingly. The parameter $\Lambda = \lambda_\perp/\lambda_\parallel$ thus defines the momentum anisotropy of the initial state.

The values of these initial state parameters are defined from the experimental data on final particle multiplicities and pion spectra. It turns out that α and Λ at the LHC remain the same at different energies of Pb + Pb collisions and various sets of other model parameters. The value $\Lambda = 100$, utilized in our study, corresponds to a very large momentum anisotropy of the initial state, typical for the CGC-based models.

After the prethermal and hydrodynamical stages, the particlization stage follows, since eventually the matter loses thermal and chemical equilibrium, the continuous medium description becomes inappropriate, and the system must be then considered as the set of hadrons. This stage is characterized by the particlization temperature T_p (close to the temperature of hadronization) which is determined by the QCD equation of state and defined as the temperature when the quark-gluon matter mostly transforms into the hadron-resonance gas.

At the last, hadronic cascade stage, the particles created during the particlization collide with each other, experiencing elastic and inelastic scatterings, and the resonance decays take place. This stage is simulated within UrQMD model [6]. Here one can allow or forbid certain decays (e.g., in order to reproduce the experimental feed-down treatment, etc.) and switch off some processes, like baryon-antibaryon annihilation, and so on.

In the article [1] it was determined that the behavior of bulk observables in iHKM depends strongly on the time of the initial state formation, τ_0. As for the relaxation time τ_{rel} and thermalization time τ_{th} characterizing the intensity of the thermalization process, this issue remained investigated insufficiently. To clarify this dependence in the current study we compare the iHKM results on the particle p_T spectra at different τ_{rel} and τ_{th}, having fixed the initial time $\tau_0 = 0.1$ fm/c and simultaneously changing the maximal initial energy density $\epsilon_0(\tau_0)$.

First, we fix the relaxation time $\tau_{\text{rel}} = 0.25$ fm/c and compare p_T spectra for main particle species, obtained in the model at the two thermalization times $\tau_{\text{th}} = 1.0$ fm/c and $\tau_{\text{th}} = 1.5$ fm/c for Pb + Pb collisions at the LHC energy $\sqrt{s_{NN}} = 2.76$ TeV. To ensure the right reproduction of the mean charged-particle multiplicity in the model for all centralities in both cases, we use two different ϵ_0 values: $\epsilon_0 = 834$ GeV/fm^3 for $\tau_{\text{th}} = 1.0$ fm/c and $\epsilon_0 = 681$ GeV/fm^3 for $\tau_{\text{th}} = 1.5$ fm/c. The corresponding results almost coincide: The comparison can be seen in Fig. 1, where the iHKM pion, kaon, and proton transverse-momentum spectra are presented for the case of $c = 0$–5% events together with the ALICE
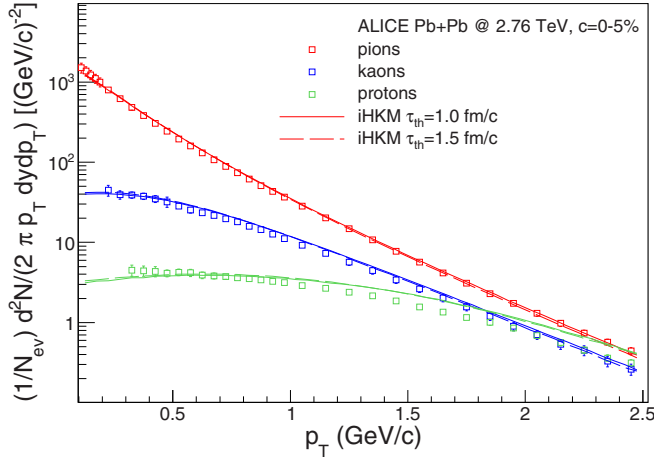
FIG. 1. The iHKM results on pion, kaon, and proton spectra in the Pb + Pb collisions with $c = 0$–5% at the LHC energy $\sqrt{s_{NN}} = 2.76$ TeV. The two different thermalization time values, $\tau_{th} = 1.0$ fm/c (solid lines) and $\tau_{th} = 1.5$ fm/c (dashed lines) were utilized. The experimental data from the ALICE Collaboration [7] are shown as square markers.

FIG. 2. The comparison of the iHKM results on pion, kaon, and proton spectra in the Pb + Pb collisions with $c = 0$–5% at the LHC energy $\sqrt{s_{NN}} = 2.76$ TeV. The two different relaxation times, $\tau_{rel} = 0.25$ fm/c (solid lines) and $\tau_{rel} = 0.60$ fm/c (dashed lines), were used. The thermalization time value in both cases was set to $\tau_{th} = 1.5$ fm/c. The experimental data measured by the ALICE Collaboration [7] are shown as square markers.

Collaboration [7] experimental data. One can notice that the slope of proton spectra obtained in iHKM is underestimated, which can be explained by strong collective flow in the model. It increases the effective temperature (inverse of the slope) of the spectra for all particle species; however, the spectra of massive particles are most sensitive to this effect, since the increase of effective temperature is roughly proportional to $mv^2/2$, where m is the particle mass and v is the root-mean-square flow velocity. Therefore the relatively high effective temperature for soft protons is, probably, due to contribution from slightly overestimated velocity gradient in the central part of the system. However, such a strong flow is necessary to correctly describe the interferometry radii in the model, as we found in the study devoted to the LHC energy 2.76A TeV [1].

In the next step, we, on the contrary, fix the value of the thermalization time at $\tau_{th} = 1.5$ fm/c and calculate the spectra at the two values of the relaxation time, $\tau_{rel} = 0.25$ fm/c and $\tau_{rel} = 0.6$ fm/c (here we choose the second τ_{rel} value to be noticeably larger than the first one, but smaller than the time of thermalization). Again, we retune also the value of
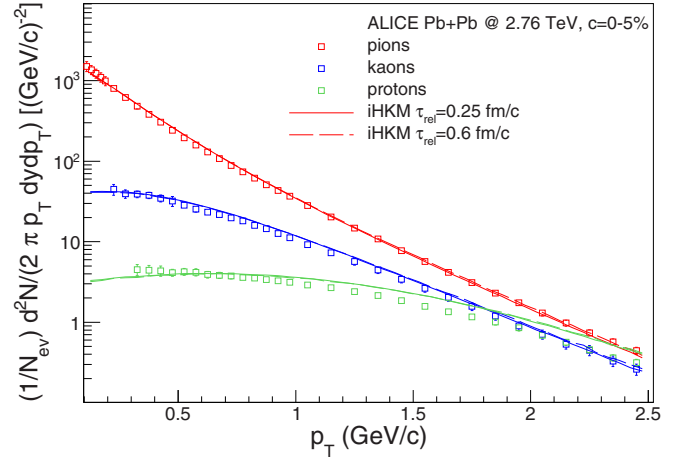
the maximal initial energy density, setting it to 630 GeV/fm^3 for the case of $\tau_{rel} = 0.6$ fm/c. Figure 2 shows the compared results for the two τ_{rel}, again together with the experimental points.

Both comparisons of the results in Figs. 1 and 2 demonstrate that while the maximal initial energy density ϵ_0 remains a free parameter, the experimentally measured p_T spectra can be successfully described at different thermalization and relaxation times, characterizing the rate of the matter's thermalization process. This fact complicates the experimental study of the process of thermalization in heavy-ion collisions.

III. RESULTS FOR $\sqrt{s_{NN}} = 5.02$ TeV AND DISCUSSION

In this section we provide the systematic study of the wide class of bulk observables at the LHC energy $\sqrt{s_{NN}} = 5.02$ TeV within iHKM using the two equations of state (EoS) for quark-gluon phase with the two corresponding particlization temperatures T_p. In Ref. [8] for the LHC energy $\sqrt{s_{NN}} = $
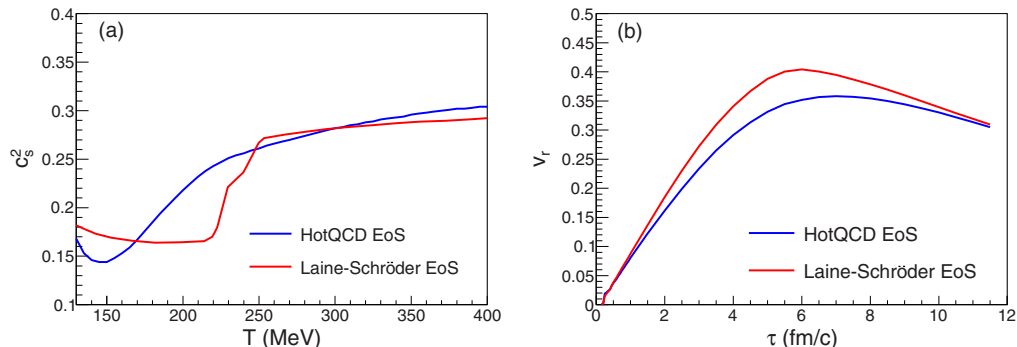

FIG. 3. The dependence of square of the speed of sound c_s^2 on the temperature T (a) and radial flow's v_r dependence on τ for $r_T = 3$ fm in iHKM (b) for Laine-Schroeder [9] and HotQCD Collaboration equations of state [10].
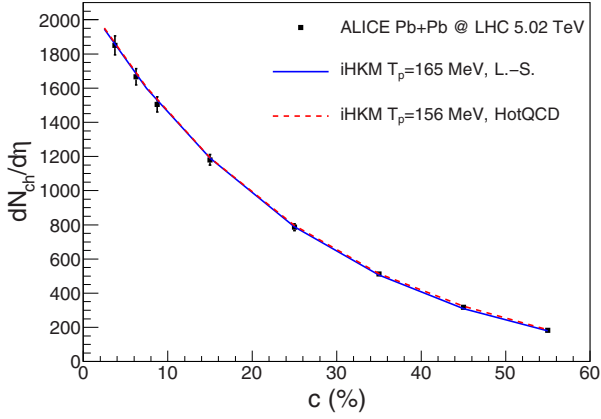
FIG. 4. The mean charged-particle multiplicity $dN_{ch}/d\eta$ dependence on collision centrality for Pb + Pb collisions at the LHC energy $\sqrt{s_{NN}} = 5.02$ TeV. The best iHKM descriptions at $T_p = 165$ MeV (with Laine-Schroeder EoS) and $T_p = 156$ MeV (with HotQCD Collaboration EoS) of the ALICE experimental data [11] are used to fix the main model parameters ϵ_0 and α in both cases.

2.76 TeV, a similar analysis was done only for particle number ratios. Here we are going to investigate whether the crucial observation made in Ref. [8], as for the possibility to get equally good data description at both EoS/T_p's if the $\epsilon_0(\tau_0)$ parameter is correspondingly adjusted, can be confirmed at higher energy and for all the observables, including not only particle yields, but also spectra, elliptic flow, femtoscopy radii, etc.

Thus, in this paper iHKM is for the first time applied to the study of collisions at the recently achieved highest LHC energy, 5.02 *A* TeV. At first, in order to adjust the model parameters to the description of Pb + Pb collisions at this new energy, we fitted the mean charged-particle multiplicity dependence on centrality and the slope of the pion p_T spectrum at the two chosen particlization temperatures and corresponding equations of state for the quark-gluon phase. We considered two cases: the particlization temperature $T_p = 165$ MeV with the Laine-Schroeder equation of state [9] and $T_p = 156$ MeV with the HotQCD Collaboration EoS [10]. For $T_p = 165$ MeV the best fit to multiplicity dependence corresponds to the value $\epsilon_0 = 1067$ GeV/fm^3 at the initial time for the system formation $\tau_0 = 0.1$ fm/c, and for $T_p = 156$ MeV the values $\epsilon_0 = 870$ GeV/fm^3 and $\tau_0 = 0.12$ fm/c are obtained from the fit. The different initial times τ_0 were used to optimize the description of pion transverse-momentum spectrum at relatively high $p_T > 1$ GeV/c. The parameter regulating the proportion between wounded nucleons and binary collisions model contributions to the initial energy density profile from GLISSANDO code [5] for both particlization temperatures is $\alpha = 0.24$—the same as for the energy $\sqrt{s_{NN}} = 2.76$ TeV.

The rest of the model parameters—the thermalization time $\tau_{th} = 1$ fm/c, the relaxation time at the prethermal stage $\tau_{rel} = 0.25$ fm/c, and the momentum anisotropy of the initial state $\Lambda = 100$—also have the values equal to those provided a successful description of Pb + Pb collision observables at $\sqrt{s_{NN}} = 2.76$ TeV [1,2].
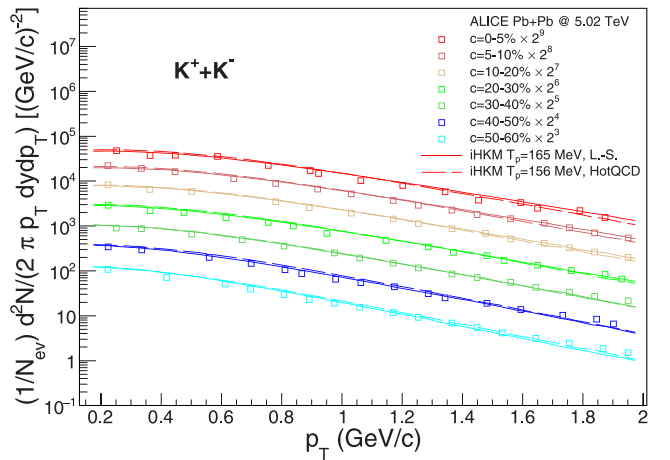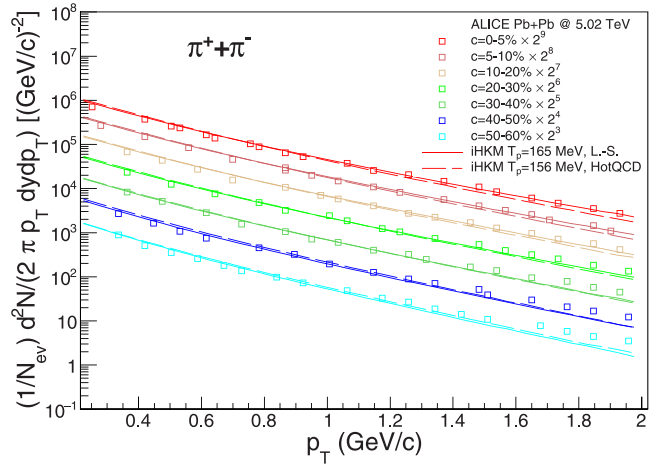

FIG. 5. Pion and kaon transverse-momentum spectra for different centrality classes obtained from iHKM at the two particlization temperatures and equations of state for quark-gluon phase in comparison with the preliminary experimental data from the ALICE Collaboration [12]. For better visibility the spectra points for different centralities are scaled by different powers of 2.

As one can see, the adjustment of iHKM to the description of collisions at new energy, 5.02 *A* TeV, is reached by natural changing of only one (!) parameter—the maximal initial energy density $\epsilon_0(\tau_0)$—as compared to that used at the previous LHC energy, 2.76 *A* TeV. This fact looks natural in case of similarity of the space-time evolution and properties of the matter at different LHC energies, and in such a case it indicates the adequacy of the model for the theoretical description of these processes.

In Fig. 3 one can see the plots, demonstrating the square of the speed of sound dependencies on temperature for both considered equations of state and the corresponding radial flow $v_r(\tau)$ evolution curves, obtained in iHKM for $r_T = 3$ fm. One can see that despite the fact that the two EoS's lead to different values of c_s^2 near the phase transition region, and hence to different matter acceleration during the hydrodynamic stage, the radial flow magnitudes, developed to system's particlization time ($\tau \approx 10$ fm/c) are quite close in both cases. This is partially due to a larger flow, developed during the early evolution stage in case of Laine-Schroeder
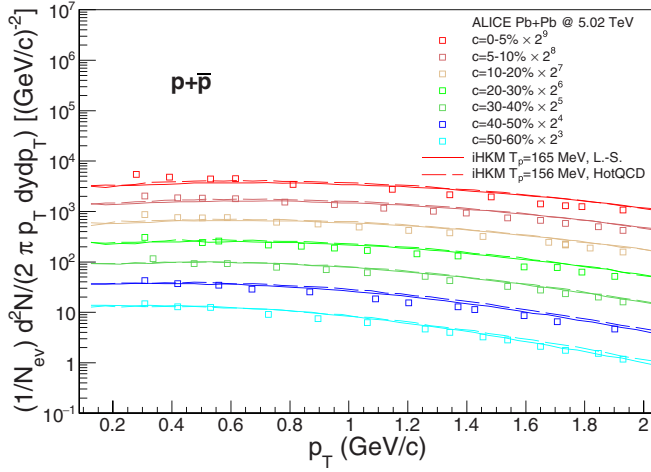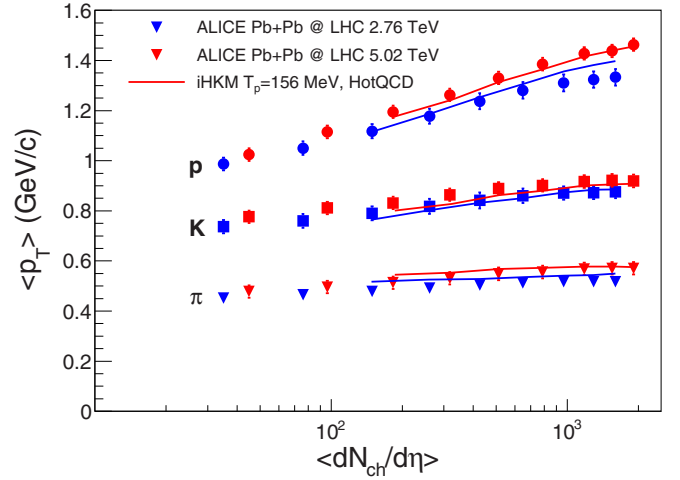
FIG. 6. The same as in Fig. 5 for protons.

FIG. 7. The iHKM results (for $T_p = 156$ MeV and HotQCD Collaboration EoS) on pion, kaon, and proton mean p_T (lines) in Pb + Pb collisions at the two LHC energies—$\sqrt{s_{NN}} = 2.76$ TeV (blue) and $\sqrt{s_{NN}} = 5.02$ TeV (red)—for different centrality classes in comparison with the ALICE Collaboration experimental data [7,12,14] (markers).

EoS, that can be connected with earlier start and essentially larger gradient of pressure in this case. At the later times, around the temperature region $170 < T < 250$ MeV, much stiffer character of HotQCD Collaboration EoS compensates the tendencies of the earlier stage.

The mean charged-particle multiplicities at different collision centralities, obtained in iHKM at chosen parameter values for $\sqrt{s_{NN}} = 5.02$ TeV Pb + Pb collisions, in comparison to the experimental data are presented in Fig. 4. At both EoS/T_p's the model reproduces the experimental dependency quite well, so that the two model curves almost coincide.

The iHKM results on transverse-momentum spectra of pions, kaons, and protons for different centralities are shown in Figs. 5 and 6. The model points are compared to the preliminary experimental data on p_T spectra measurement, presented at Quark Matter 2017 [12]. As one can see, iHKM gives a satisfactory description of the particle production for the $\sqrt{s_{NN}} = 5.02$ TeV Pb + Pb collisions in both T_p/EoS modes. It is worth noting that the pion spectra in iHKM model are described within the experimental errors in a wide-p_T region including the soft momentum interval. Previously, a similar result was observed and emphasized in Ref. [2] for the LHC energy $\sqrt{s_{NN}} = 2.76$ TeV. Therefore, in iHKM there is no necessity to include a specific mechanism for soft pion radiation, for example, through the Bose-Einstein condensation [13], in order to describe the soft pion emission in Pb + Pb collisions at the LHC.

In addition, in Fig. 7 we demonstrate the iHKM results for mean transverse momentum of pions, kaons, and protons for seven centrality classes at the two collision energies, $\sqrt{s_{NN}} = 2.76$ TeV and $\sqrt{s_{NN}} = 5.02$ TeV, compared with the ALICE Collaboration experimental points [7,12,14]. We see that in the main iHKM points agree with the data, in particular the model reproduces a certain (up to 8–10%) increase of mean p_T values at 5.02 A TeV against 2.76A TeV, although at 2.76A TeV the model slightly overestimates pion $\langle p_T \rangle$ and proton $\langle p_T \rangle$ in central events, while kaon mean p_T are slightly underestimated at 5.02 A TeV in peripheral events.

In Fig. 8 one can see the p_T-integrated particle yields dN/dy for different species, calculated in the model in com-

parison with the preliminary experimental data, provided by the ALICE Collaboration and reported in the talk at Quark Matter 2018 [15].

In Fig. 9 we demonstrate the results of iHKM simulations for the various particle number ratios in central Pb + Pb collisions ($c = 0$–10%) at the considered LHC energy again together with the preliminary experimental results from the ALICE Collaboration [15], obtained by division of the corresponding experimental particle yields shown in Fig. 8. Here the model ratios obtained from the full iHKM calculations are presented along with those calculated in the mode with inelastic reactions turned off. As one can see, while the results
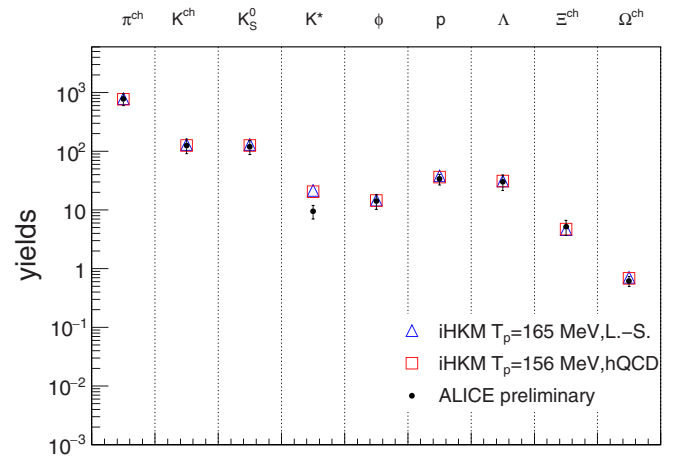

FIG. 8. Particle yields dN/dy in 5.02-A TeV events with $c = 0$–10% calculated in iHKM at the two particlization temperatures and equations of state ($T_p = 165$ MeV with Laine-Schroeder EoS and $T_p = 156$ MeV with HotQCD Collaboration EoS) compared to the preliminary ALICE data [15].
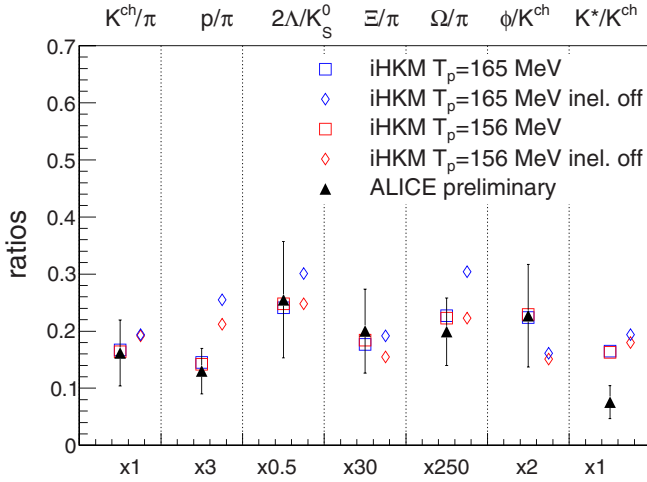
FIG. 9. The iHKM results for the particle number ratios calculated at the two particlization temperatures and quark-gluon matter equations of state ($T_p = 165$ MeV with Laine-Schroeder EoS and $T_p = 156$ MeV with HotQCD Collaboration EoS) for 5.02 A TeV collisions with $c = 0$–10% compared to the preliminary ALICE data [15]. The simulations are performed in two regimes: the full one and the one with inelastic processes turned off.
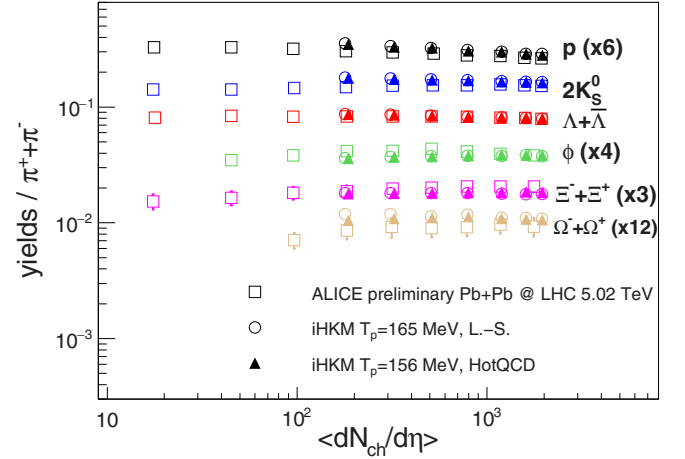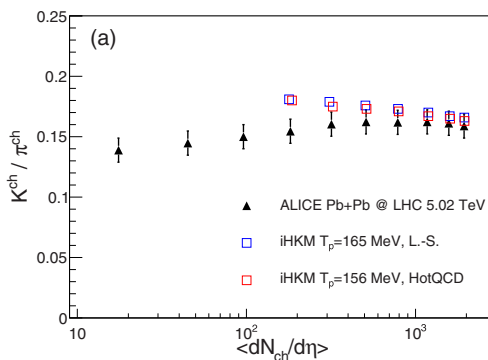

FIG. 11. The iHKM results on the ratios of different particle yields to the pion yield at different collision centralities for the LHC Pb + Pb collisions at $\sqrt{s_{NN}} = 5.02$ TeV together with the preliminary ALICE Collaboration data [17].

for certain ratios in the latter "reduced" mode can noticeably differ for the two particlization temperatures, the full calculation always gives very close values in both cases. This peculiarity in results is in accordance with that observed and discussed in our previous work [8]. The compensatory mechanism, eliminating in the "full" mode the difference, observed between the ratios at the two EoS/T_p's in the "reduced" mode, is associated with inelastic reactions in the hadronic cascade, which last longer at a higher particlization temperature. The full mode iHKM results are in good agreement with the data, except for the K^*/K ratio. The latter detail is unexpected and needs specific discussion.

Turning back to the Fig. 8, one sees that the latter discrepancy is due to overestimation of the K^* yield in the model—its value is approximately twice higher in iHKM than in the experiment. This fact looks strange, since in our

recent study [8], focused on the particle production in the LHC Pb + Pb collisions at lower energy, $\sqrt{s_{NN}} = 2.76$ TeV, we obtained a good agreement between model K^* yield (and K^*/K ratio) description and the corresponding ALICE data. Note that in our simulations we accounted also for possible problems with the K^* identification through the products of its decay into kaons and pions, which could be caused by the interaction of these daughter particles with the surrounding hadronic medium. This issue was analyzed in detail in another our paper [16]. There we considered the case of Pb + Pb collisions at the LHC at $\sqrt{s_{NN}} = 2.76$ TeV and performed the simulations in iHKM, applying the experimental procedure of K^* identification, i.e., selecting the $K\pi$ pairs, emitted from the close space points and having the specific invariant mass, corresponding to $K^*(892)$ resonance. Then we compared in such a way obtained K^* yields with the full numbers of K^*, generated in the model during the hadronization of continuous quark-gluon medium. We found that the observed number of K^* resonances, reconstructed via the products of their decays, for the most central events can be up to 20% less
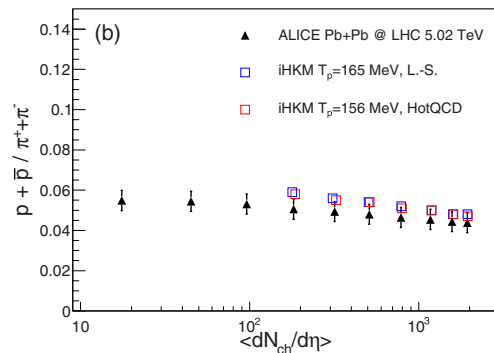

FIG. 10. The iHKM results for the K/π (a) and p/π (b) particle number ratios' dependence on mean charged-particle multiplicity calculated at the two particlization temperatures and equations of state ($T_p = 165$ MeV with Laine-Schroeder EoS and $T_p = 156$ MeV with HotQCD Collaboration EoS) and the corresponding experimental data [12] for $\sqrt{s_{NN}} = 5.02$ TeV.
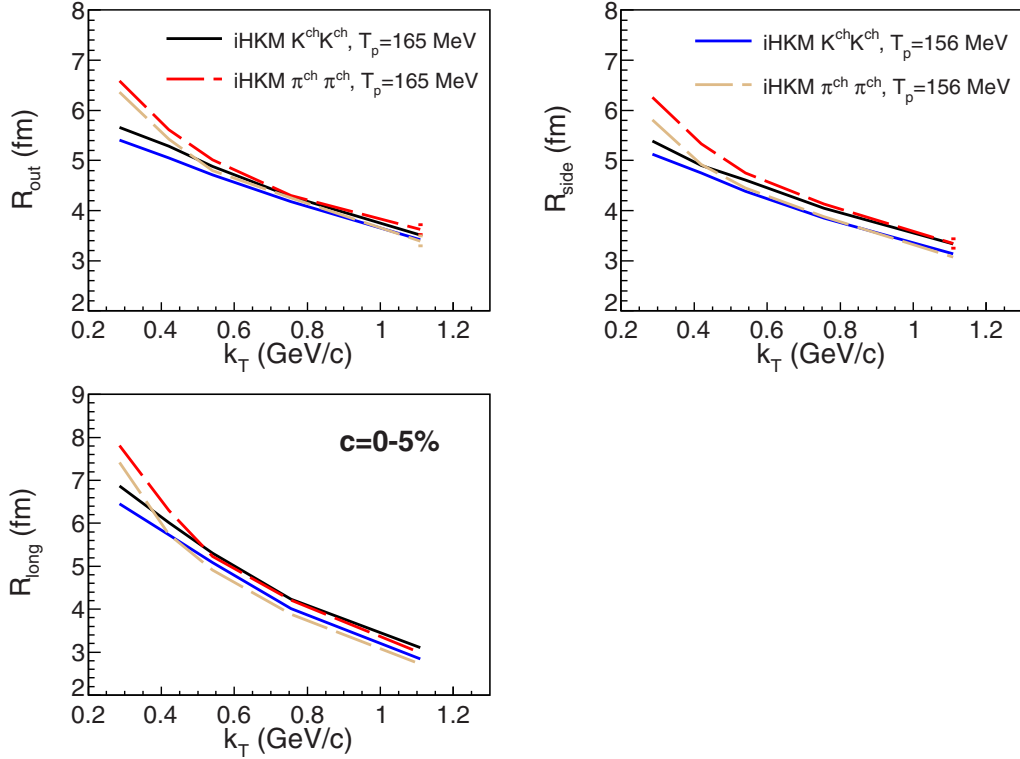
FIG. 12. The iHKM prediction for the charged pion and kaon interferometry radii k_T dependence in the LHC Pb + Pb collisions at $\sqrt{s_{NN}} = 5.02$ TeV, $c = 0$–5%. The calculations were performed at the two particlization temperatures and equations of state for quark-gluon matter ($T_p = 165$ MeV with Laine-Schroeder EoS and $T_p = 156$ MeV with HotQCD Collaboration EoS).

than the actual number of "primary" K^*'s. But it is worth noting that the mentioned reduction is a result of interplay of two opposite processes—the scattering of daughter K and π, resulting in an impossibility to detect the respective parent K^*'s (this affects up to 70% of direct resonances), and the recombination of $K\pi$ pairs, producing additional K^* resonances (this mechanism can give up to 50% of the initial number of direct K^*'s). Both these processes in iHKM are simulated at its final "afterburner" stage within the UrQMD model.

What is interesting, in the present study we apply the same K^* restoration procedure, but this time obtain a higher dN/dy, than in the data (note also that this preliminary experimental dN/dy value for K^* at $\sqrt{s_{NN}} = 5.02$ TeV is noticeably smaller than that at $\sqrt{s_{NN}} = 2.76$ TeV, while the iHKM results at both collision energies are close). The reason for a low value of K^* yield in the preliminary experimental results is unclear and needs further investigation. It can be possibly explained by the identification problems in the experiment and one cannot exclude that the dN/dy value for K^* can be corrected in the final version of ALICE data.

For the K/π and p/π ratios we have also studied within iHKM their dependence on the mean charged-particle multiplicity for different centrality classes and compared the simulation results to the preliminary experimental data, presented in Ref. [12] (see Fig. 10). In the plot one can see that the model describes well both ratios' behavior in not-far-from-central

events at both EoS/T_p's.[1] An equally good agreement of iHKM results with the data can be observed in Fig. 11, where the model calculations of the ratios of various particle species yields to the pion yield are compared to the preliminary experimental points from the ALICE Collaboration [17].

In Figs. 12–14 we demonstrate our predictions for the 5.02 A TeV pion and kaon interferometry radii $R_{\rm out}$, $R_{\rm side}$, and $R_{\rm long}$ measured at different mean pair transverse momentum k_T. The predictions are provided for the three centrality classes: $c = 0$–5%, $c = 20$–30%, and $c = 40$–50%. The radii behavior for each particle species looks regular and quite similar to that observed at lower LHC energy, 2.76 A TeV (see comparison for $c = 0$–5% in Fig. 15). The radii's absolute values are close at both energies (some values at 5.02 A TeV are slightly higher, about 3–5%) and, as expected, show a decrease when going from central to noncentral events. The similarity of the radii at both LHC energies, observed despite the different geometric sizes of the systems at freeze-out stage, is conditioned by higher velocity gradients at larger energies that compensate the geometric effects and lead to closeness of the homogeneity lengths in both cases [18].

---

[1]Here the "full regime" calculations are implied. The theoretical values obtained in the "reduced regime" without inelastic scatterings are not expected to describe the measured data. Their calculated values are fairly larger than the measured ones and for this reason are not shown on the plots in Figs. 10 and 11.
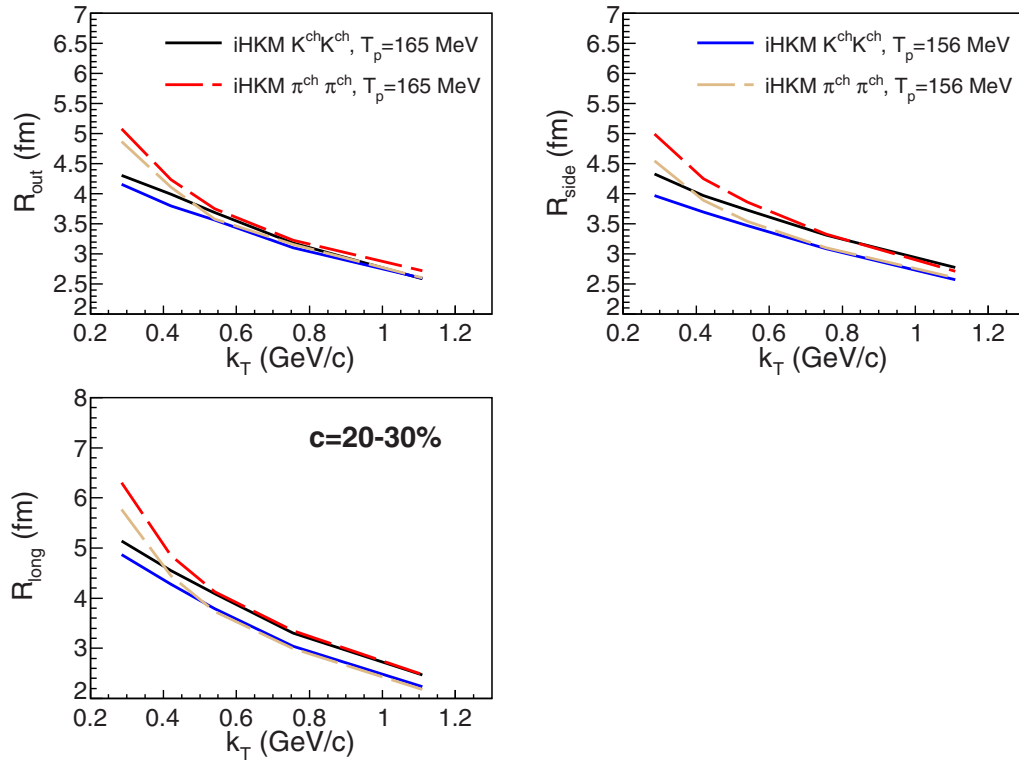
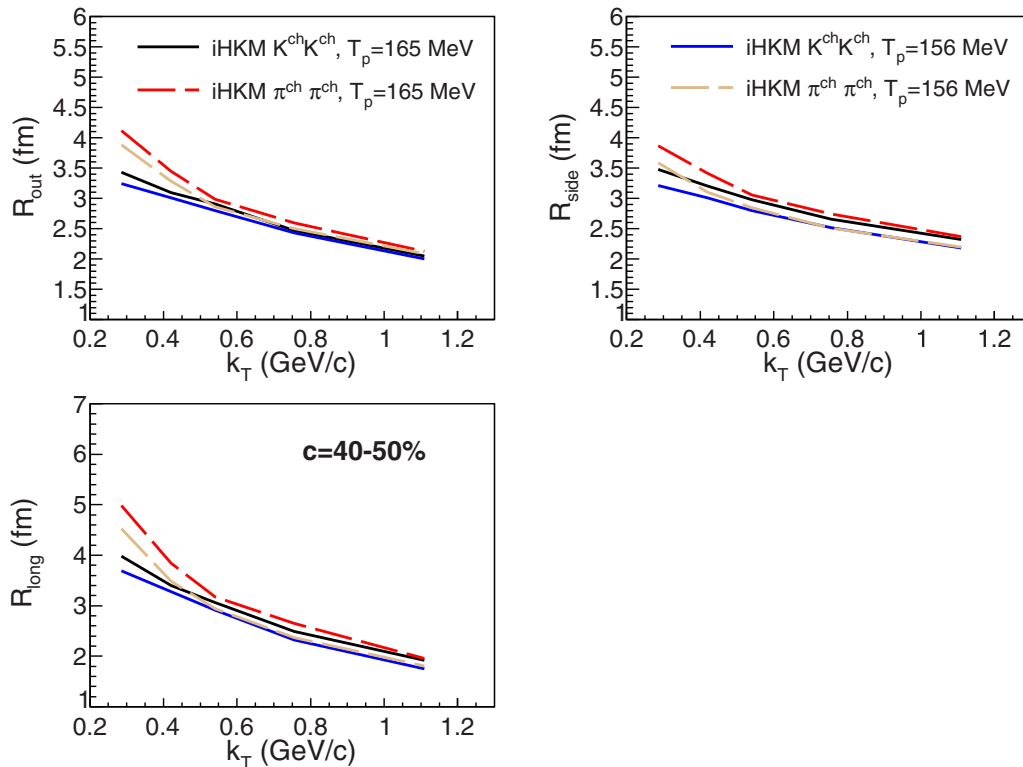FIG. 13. The same as in Fig. 12 for the centrality $c = 20$–30%.

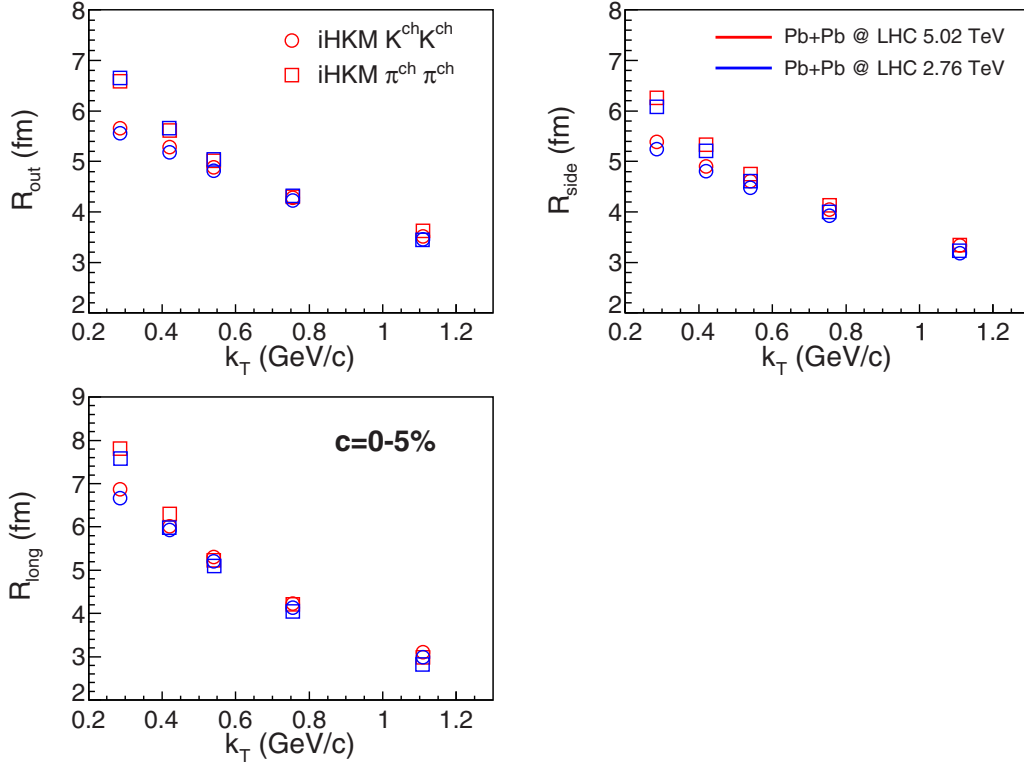FIG. 14. The same as in previous two figures for the centrality $c = 40$–50%.

FIG. 15. The comparison of iHKM results ($T_p = 165$ MeV, Laine-Schroeder EoS) for pion and kaon interferometry radii at the two LHC energies, $\sqrt{s_{NN}} = 2.76$ TeV and $\sqrt{s_{NN}} = 5.02$ TeV, centrality $c = 0$–5%.

Comparing kaon and pion points, one can see the approximate k_T scaling between two dependencies at $k_T > 0.4$ GeV/c, repeating the behavior observed for the collisions at $\sqrt{s_{NN}} = 2.76$ TeV and noticed in iHKM simulations [19] prior to the experimental confirmation in Ref. [20].

In Figs. 16 and 17 for the two centrality classes one can see the comparison of iHKM results on the all charged particles flow harmonics $v_2(p_T)$, $v_3(p_T)$, and $v_4(p_T)$ with the ALICE experimental data for $\sqrt{s_{NN}} = 5.02$ TeV [21]. Note, however, that while in the ALICE paper $v_n(p_T)$ were calculated using the two-particle cumulant method, in our analysis we use the standard event-plane method (see, e.g., Refs. [22,23]).

Following the event-plane method procedure, we at first calculate for each analyzed event the event-plane angles Ψ_n, using their relations with the event flow vectors $\mathbf{Q}_n$:

$$Q_n \cos(n\Psi_n) = \sum_i w_i \cos(n\phi_i), \tag{6}$$

$$Q_n \sin(n\Psi_n) = \sum_i w_i \sin(n\phi_i), \tag{7}$$

which give us

$$\Psi_n = \frac{1}{n} \tan^{-1} \frac{\sum_i w_i \sin(n\phi_i)}{\sum_i w_i \cos(n\phi_i)}. \tag{8}$$

Here i numerates the analyzed particles (we select particles with p_T from the range $0.2 < p_T < 2.4$ GeV/c for the analysis), and w_i is the weight of ith particle. In our study w_i are chosen to equal the particle transverse momentum $p_{T,i}$.

The flow harmonics $v_n(p_T)$ are calculated as follows:

$$v_n(p_T) = \langle \cos[n(\phi_i - \Psi_n)]\rangle / R_n, \tag{9}$$

where angle brackets mean the averaging over all the analyzed particles in considered p_T bin and $R_n = \langle \cos[n(\Psi_n - \Psi_{\mathrm{RP}})]\rangle$
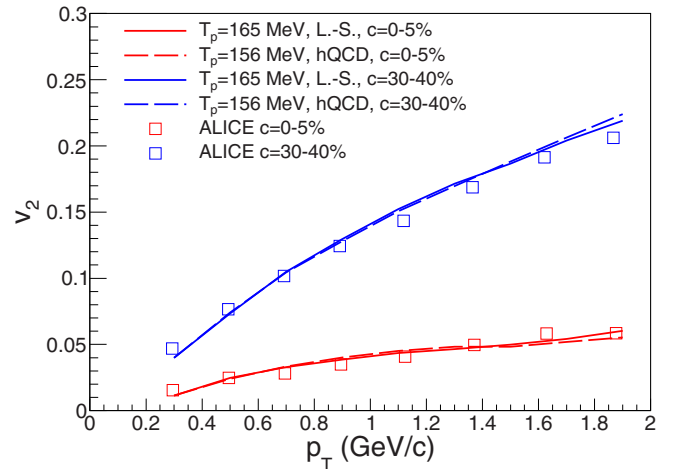

FIG. 16. The iHKM results on the elliptic flow v_2 dependence on p_T for all charged particles together with the corresponding ALICE data [21] for the centrality classes $c = 0$–5% and $c = 30$–40%. The model curves for the two particlization temperatures and the corresponding equations of state ($T_p = 165$ MeV with Laine-Schroeder EoS and $T_p = 156$ MeV with HotQCD Collaboration EoS) are presented.
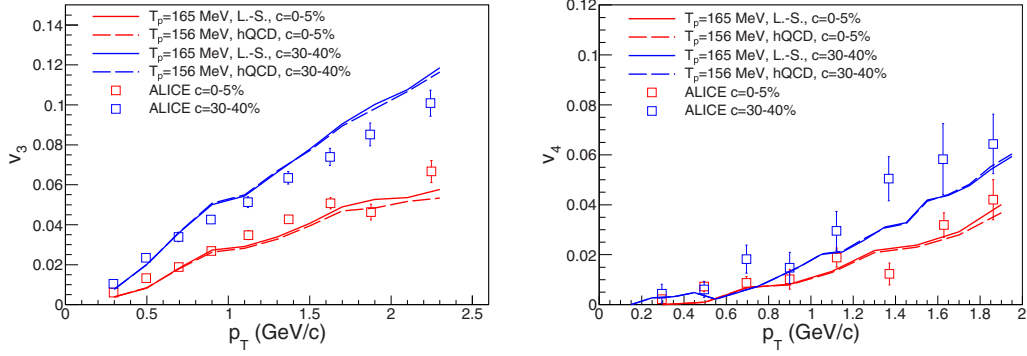
FIG. 17. The same as in Fig. 16 for v_3 and v_4 flow harmonics.

is the event-plane resolution, with Ψ_{RP} being the reaction plane angle. The event-plane resolution can be expressed through the resolution parameter χ_n as [22]

$$R_n(\chi_n) = \frac{\sqrt{\pi}}{2\sqrt{2}} \chi_n \exp\left(-\chi_n^2/4\right)\left[I_0\left(\chi_n^2/4\right) + I_1\left(\chi_n^2/4\right)\right]. \tag{10}$$

Here I_k denotes the modified Bessel function of order k and $\chi_n = v_n/\sigma$, where σ characterizes the variance of $n(\Psi_n - \Psi_{RP})$ distribution. To estimate the event-plane resolution we divide each event into two subevents with equal multiplicities and calculate the subevent value $R_n^{sub} = \sqrt{\langle \cos[n(\Psi_n^A - \Psi_n^B)]\rangle}$. After that we numerically solve (10) with respect to χ_n and obtain the subevent resolution parameter χ_n^{sub}. The full event-plane resolution R_n is then calculated using (10) as $R_n(\sqrt{2}\chi_n^{sub})$, since the particle number in full event is twice bigger than that in each subevent and χ_n is proportional to the square root of particle number.

Examining the iHKM results, presented in Figs. 16 and 17, one can notice that the model curves for the two equations of state and particlization temperatures almost coincide. The v_2 iHKM points are in good agreement with data for both centralities. As for v_3 and v_4, the iHKM describes well the central collision measurements, and for the $c = 30$–40% model gives a satisfactory data description only at $p_T < 1$ GeV/c. The statistical errors for all the presented theoretical $v_n(p_T)$ points are less than 2%. The results for the LHC energy $\sqrt{s_{NN}} = 2.76$ TeV are quite close to those for $\sqrt{s_{NN}} = 5.02$ TeV, especially in the "soft" p_T region, $p_T < 2.5$ GeV/c, both in the experiment and in the model calculations, so we demonstrate here only the 5.02-A TeV results.

As one can see, the iHKM results on all the considered bulk observables at the two particlization temperatures and corresponding equations of state are close to each other, which means that when constructing the model for a high-energy collision process, one has a certain freedom in choosing the equation of state, particlization temperature T_p, and maximal initial energy density $\epsilon_0(\tau_0)$, since different combinations of these parameter choices give similar results. This also means that experimentally one is hardly able to strictly define each of these parameters separately basing on the considered observables.

Thus, the obtained results for Pb + Pb collisions at $\sqrt{s_{NN}} = 5.02$ TeV allow us to confirm and extend an impor-

tant conclusion, made in Ref. [8] basing only on the analysis of particle number ratios at $\sqrt{s_{NN}} = 2.76$ TeV—the multiple hadronic rescatterings at the final stage of the collision play a vital role in formation of all the bulk observables and compensate the changes introduced to the system's evolution by switching to another EoS for (quasi)thermalized matter, used at the hydrodynamic stage, and another hadronization temperature.

IV. CONCLUSIONS

The theoretical predictions and the description of the preliminary experimental results for bulk observables in Pb + Pb collisions at the LHC energy $\sqrt{s_{NN}} = 5.02$ TeV within iHKM model are presented. The model parameters are the same as at simulations of 2.76-A TeV Pb + Pb collisions, except for the maximal initial energy density $\epsilon_0(\tau_0)$, appearing to be the only parameter that needed retuning. This justifies the utilization of iHKM for the description of high-energy heavy-ion collisions and confirms that it provides an adequate approach to the simulation of such processes.

The systematic study of a large set of bulk observables (particle yields, particle number ratios, p_T spectra, v_n coefficients, femtoscopy radii) was performed using the two different particlization temperatures associated with two corresponding equations of state for quark-gluon phase. The comparison of the obtained results in these cases shows that both T_p/EoS can provide an equally good description of measured data and quite close predictions for not-yet-measured observables, if having changed the T_p and EoS, one simultaneously readjusts the maximal initial energy density parameter $\epsilon_0(\tau_0)$.

This result confirms our previous observation [8] for particle number ratios in Pb + Pb collisions at lower LHC energy $\sqrt{s_{NN}} = 2.76$ TeV and supports the conclusion about the great importance of the final afterburner stage of the collision and intensive hadron interactions, taking place at this stage, for the formation of the observed results. It means, however, that the matter EoS at the hydrodynamic stage and the particlization temperature cannot be strictly constrained by the experimental data.

Among the obtained results one can highlight an unexpectedly low value of $K^*(892)$ yield in the preliminary experimental data, as compared to the iHKM result and the

previous ALICE result for $\sqrt{s_{NN}} = 2.76$ TeV collisions. We associate this discrepancy with imperfection of preliminary experimental data analysis and believe that eventually it can likely be eliminated in the final version of ALICE data.

Also, the simulation results' dependence on such characteristics of the prethermal stage of matter evolution as the thermalization time τ_{th} and relaxation time τ_{rel} is investigated for the LHC energy $2.76\,A$ TeV. In this article we demonstrate that varying these parameters in quite wide ranges (1–1.5) fm/c for τ_{th} and (0.25–0.6) fm/c for τ_{rel} accompanied again by the corresponding change of $\epsilon_0(\tau_0)$ does not influence the final particle p_T spectra. Thus, one may assume that some important characteristics of the matter and its evolution in $A + A$ collisions cannot be unambiguously extracted from the experimental results if the maximal initial energy density (or—in other than iHKM kinds of approaches—a combination of some other model parameters that set the initial energy)

can be considered an (effective) free parameter. The situation could become more clear when the dynamical mechanism of loosely bound objects formation [24] in nuclear collisions becomes clarified and incorporated into evolutionary models like iHKM.

[1] V. Yu. Naboka, Iu. A. Karpenko, and Yu. M. Sinyukov, Phys. Rev. C **93**, 024902 (2016).

[2] V. Yu. Naboka, S. V. Akkelin, Iu. A. Karpenko, and Yu. M. Sinyukov, Phys. Rev. C **91**, 014906 (2015).

[3] S. V. Akkelin and Yu. M. Sinyukov, Phys. Rev. C **81**, 064901 (2010).

[4] J. D. Bjorken, Phys. Rev. D **27**, 140 (1983).

[5] W. Broniowski, M. Rybczynski, and P. Bozek, Comput. Phys. Commun. **180**, 69 (2009).

[6] S. A. Bass *et al.*, Prog. Part. Nucl. Phys. **41**, 255 (1998); M. Bleicher *et al.*, J. Phys. G **25**, 1859 (1999).

[7] B. Abelev *et al.* (ALICE Collaboration), Phys. Rev. C **88**, 044910 (2013).

[8] Yu. M. Sinyukov and V. M. Shapoval, Phys. Rev. C **97**, 064901 (2018).

[9] M. Laine and Y. Schroder, Phys. Rev. D **73**, 085009 (2006).

[10] A. Bazavov, T. Bhattacharya, C. DeTar, H. T. Ding, S. Gottlieb, R. Gupta, P. Hegde, U. M. Heller, F. Karsch, E. Laermann, L. Levkova, S. Mukherjee, P. Petreczky, C. Schmidt, C. Schroeder, R. A. Soltz, W. Soeldner, R. Sugar, M. Wagner, and P. Vranas (The HotQCD Collaboration), Phys. Rev. D **90**, 094503 (2014).

[11] J. Adam *et al.* (ALICE Collaboration), Phys. Rev. Lett. **116**, 222302 (2016).

[12] N. Jacazio (for the ALICE Collaboration), Nucl. Phys. A **967**, 421 (2017).

[13] V. Begun and W. Florkowski, Phys. Rev. C **91**, 054909 (2015).

[14] M. Petrovici, A. Lindner, A. Pop, M. Tarzila, and I. Berceanu, Phys. Rev. C **98**, 024904 (2018).

[15] F. Bellini (for the ALICE Collaboration), Nucl. Phys. A **982**, 427 (2019).

[16] V. M. Shapoval, P. Braun-Munzinger, and Yu. M. Sinyukov, Nucl. Phys. A **968**, 391 (2017).

[17] D. S. D. Albuquerque (for the ALICE Collaboration), Nucl. Phys. A **982**, 823 (2019).

[18] S. V. Akkelin and Yu. M. Sinyukov, Phys. Lett. B **356**, 525 (1995); Yu. M. Sinyukov, Nucl. Phys. A **566**, 589 (1994).

[19] V. M. Shapoval, P. Braun-Munzinger, Iu. A. Karpenko, and Yu. M. Sinyukov, Nucl. Phys. A **929**, 1 (2014).

[20] S. Acharya *et al.* (ALICE Collaboration), Phys. Rev. C **96**, 064613 (2017).

[21] J. Adam *et al.* (The ALICE Collaboration), Phys. Rev. Lett. **116**, 132302 (2016).

[22] A. M. Poskanzer and S. A. Voloshin, Phys. Rev. C **58**, 1671 (1998).

[23] S. A. Voloshin, A. M. Poskanzer, R. Snellings, in *Landolt-Börnstein—Group I Elementary Particles, Nuclei and Atoms 23 (Relativistic Heavy Ion Physics)*, edited by R. Stock (Springer-Verlag, Berlin, 2010).

[24] P. Braun-Munzinger and B. Dönigus, Nucl. Phys. A **987**, 144 (2019).